Published in final edited form as:
Cell Stem Cell. 2012 March 2; 10(3): 259–272. doi:10.1016/j.stem.2012.02.003.

Endogenous Bone Marrow MSCs Are Dynamic, Fate-Restricted Participants in Bone Maintenance and Regeneration

Dongsu Park[1,4,6], **Joel A. Spencer**[2,4], **Bong Ihn Koh**[1,4], **Tatsuya Kobayashi**[3], **Joji Fujisaki**[2,4], **Thomas L. Clemens**[5], **Charles P. Lin**[2,4], **Henry M. Kronenberg**[3], and **David T. Scadden**[1,4,6,*]

[1]Center for Regenerative Medicine, Massachusetts General Hospital, 185 Cambridge Street, Boston, MA 02114, USA

[2]Advanced Microscopy Program, Wellman Center for Photomedicine and Center for Systems Biology, Massachusetts General Hospital, 185 Cambridge Street, Boston, MA 02114, USA

[3]Endocrine Unit, Massachusetts General Hospital, 185 Cambridge Street, Boston, MA 02114, USA

[4]Harvard Stem Cell Institute, 1350 Massachusetts Avenue, Cambridge, MA 02138, USA

[5]Center for Musculoskeletal Research, Johns Hopkins Medicine, 601 North Caroline Street, Baltimore, MD 21287, USA

[6]Department of Stem Cell and Regenerative Biology, Harvard University, 7 Divinity Avenue, Cambridge, MA 02138, USA

SUMMARY

Mesenchymal stem cells (MSCs) commonly defined by in vitro functions have entered clinical application despite little definition of their function in residence. Here, we report genetic pulse-chase experiments that define osteoblastic cells as short-lived and nonreplicative, requiring replenishment from bone-marrow-derived, *Mx1*$^{+}$ stromal cells with “MSC” features. These cells respond to tissue stress and migrate to sites of injury, supplying new osteoblasts during fracture healing. Single cell transplantation yielded progeny that both preserve progenitor function and differentiate into osteoblasts, producing new bone. They are capable of local and systemic translocation and serial transplantation. While these cells meet current definitions of MSCs in vitro, they are osteolineage restricted in vivo in growing and adult animals. Therefore, bone-marrow-derived MSCs may be a heterogeneous population with the *Mx1*$^{+}$ population, representing a highly dynamic and stress responsive stem/progenitor cell population of fate-restricted potential that feeds the high cell replacement demands of the adult skeleton.

INTRODUCTION

Complex multicellular organisms depend on mesenchymal cells to provide an architectural superstructure for the body whole and the organs within it. Yet, a detailed understanding of these cells is very limited for most tissues with the exception of the musculoskeletal system. There, it is apparent that subpopulations of mesenchymal cells provide specific functional

*Correspondence: david_scadden@harvard.edu.

SUPPLEMENTAL INFORMATION

Supplemental Information for this article includes seven figures and Supplemental Experimental Procedures and can be found with this article online at doi:10.1016/j.stem.2012.02.003.

roles, including osteolineage cell participation in bone maintenance, bone marrow function, and metabolic regulation (Lee et al., 2007; Raaijmakers et al., 2010).

The existence of multipotent bone marrow stromal cells (BMSCs), or skeletal/mesenchymal stem cells (SSCs/MSCs, hereafter MSCs) was proposed based on the identification of clonogenic populations within the bone marrow that could differentiate into osteoblasts, chondrocytes, and adipocytes ex vivo (Caplan, 1991; Friedenstein et al., 1974) and, in some cases, recapitulate bone and marrow formation upon transplantation of cultured cells (Sacchetti et al., 2007). Similar multipotent MSCs can be isolated from mouse bone marrow (Morikawa et al., 2009) or from multiple tissue types in human (Crisan et al., 2008). These isolated populations have entered clinical testing to either replace cells in damaged tissues or provide paracrine signals to modulate injury or immune responses. However, how such cells perform in vivo and how they contribute to the homeostasis of tissues in situ remains poorly understood, and therefore, in vivo clonal analysis of endogenous MSCs is required.

Cell replacement under homeostatic conditions or after injury is controlled either by symmetric division of existing mature cells (Dor et al., 2004) or by differentiation of stem/progenitor cells (Li and Clevers, 2010). The existence of stem or progenitor cell populations that can generate skeletal tissues in vivo has been documented by transplantation of MCAM/CD146^{+} subendothelial cells from human bone marrow (Sacchetti et al., 2007) or CD105^{+}Thy1^{-} cells from mouse fetal bone (Chan et al., 2009) and by lineage tracing of nestin^{+} bone marrow cells (Méndez-Ferrer et al., 2010). Yet, which osteolineage cells divide and contribute to skeletal remodeling and repair is unclear. Some studies indicate that bone-surface osteoblasts are postmitotic and replaced by unspecified immature cells (Kalajzic et al., 2008; McCulloch and Heersche, 1988; Owen and MacPherson, 1963), while in development, osteoblasts divide (Dominici et al., 2009; Maes et al., 2010). Further, blood-borne cells contributing to bone repair have been suggested by reports of circulating osteoblasts (Eghbali-Fatourechi et al., 2005; Otsuru et al., 2008). Therefore, the dynamics of osteolineage cells in adult animals is an issue of debate.

Population dynamics is of particular interest given recent findings that osteolineage cells, when perturbed, can result in conditions of disorganization of the hematopoietic system, including myelodysplasia and acute myeloid leukemia (Raaijmakers et al., 2010; Walkley et al., 2007a). These models suggest that genetic alterations in the microenvironment can be an initiating lesion in the multistep pathway to cancer, at least in the bone marrow (Raaijmakers et al., 2010). If osteolineage cells are long-lived and replace themselves, such a model would be less likely. In contrast, a stem/progenitor population replenishing short-lived mature cells could provide the scenario for acquired genetic lesions to affect a larger pool of microenvironmental cells, particularly if such cells were capable of translocation. Here, we define that the latter conditions describe the kinetics and functional properties of osteolineage cells in adult mice using engineered strains that enable marking of specific cells types, including the putative MSC.

RESULTS

Pulse-Chase of Mature Osteoblasts In Vivo

To study the kinetics and fate of functional mature cells, we used a mouse with the mature osteoblast specific gene, *osteocalcin* (Ocn) (Ducy et al., 1996), driving a Cre recombinase and modified estrogen receptor (ER) fusion gene. These mice were crossed with *ROSA26-loxP-stop-loxP-EYFP* (herein *Rosa-YFP*) reporter mice to generate *Ocn-Cre-ER*$^{+}$*Rosa-YFP*$^{+}$ (herein iOcn) mice (Figure 1A) where Cre recombinase could be activated in a cell-stage- and time-dependent manner, the latter by administration of 4-hydroxytamoxifen (4-OHT). We administered 4-OHT to 6- to 8-week-old mice, resulting in *loxP*-flanked stop

sequence deletion and the constitutive expression of the YFP reporter gene in mature osteoblasts and their progeny. Immunohistochemistry for the reporter detected distinct and quantifiable YFP^+ osteoblasts on the endosteal and periosteal surfaces of femurs and calvaria from iOcn reporter mice at 14 days after only two doses of 4-OHT treatment (Figure S1A available online), confirming the efficiency of our system.

Rapid Turnover of Mature Osteoblasts In Vivo

Intravital, two-photon/confocal hybrid microscopy was used to visualize, quantify, and track the position of Ocn/YFP^+ osteoblasts in live animals (Lo Celso et al., 2009) (Figure 1A). Fourteen days after 4-OHT treatment, we scanned both sides of the sagittal (S.S.) and coronal (C.S.) sutures, which permitted examination of 40%–60% of the calvarial cavities of the mouse (Sipkins et al., 2005) (Figure 1B, left panel). We detected quantifiable YFP^+ osteoblasts distinct from bone matrix (blue; by second harmonic generation) and vasculature (red; Q-dot) (Figures 1B [right] and S1B). To trace the same cells over time, we selected a specific region based on invariant suture landmarks and mapped this cavity using four to six consecutive images with Z-stacks (Figure 1B, L1–L4), sequentially imaging individual iOcn mice over a 6-month period. Without 4-OHT treatment, very low or no detectable YFP^+ osteoblasts were detected (1.75 ± 1.5 cells in 660 μm^2) (Figure 1C, $n = 4$). We found a peak YFP-labeling of endosteal osteoblasts at 14 days (118 ± 31.4 in 660 μm^2, $n = 6$), followed by a significant decrease to ~50% by 30 days ($p < 0.0001$), eventually reaching the basal level by 60 days (Figures 1C, 1D, and S1C). 3D reconstruction of the Z-stack images showed that the majority of YFP^+ osteoblasts were individually and discontinuously distributed along the endosteal surface without clustering (Figure 1C, bottom). (Note, microvessels vary because the exposure of the skull for imaging leads to wound responses.) Immunohistochemistry of selected bones imaged above at day 14 and day 60 confirmed the results of the in vivo imaging (Figure S1D). In contrast to osteoblasts, small, bone-embedded YFP^+ osteocytes peaked in number at 30 days after 4-OHT treatment and then decreased over time, consistent with existing paradigms whereby some mature osteoblasts differentiate into osteocytes (Dallas and Bonewald, 2010) (Figure 1E). Histology of femurs and calvaria also confirmed the decrease in labeled endosteal and periosteal osteoblasts, consistent with intravital microscopy (Figures S1D and S1E).

Despite the continuous decrease in number of Ocn/YFP^+ osteoblasts, it could be possible that mature osteoblasts proliferate early after tamoxifen induction. Therefore, we performed anti-Ki-67 immunohistochemistry with calvarial bones at day 4 and day 7 after 4-OHT treatment because efficient YFP labeling begins 2–3 days after tamoxifen induction. In all time points examined (day 14, data not shown), there was no observable Ki-67 staining in these cells ($n > 200$ counted, Figure 1F), demonstrating that existing osteoblasts turn over rapidly and are continuously replaced by another cell population. Independent experiments using BrdU uptake confirmed these results (Figure S1F).

Because mature osteoblasts were reported to proliferate in irradiated bones (Dominici et al., 2009), we next examined whether a distinct type of injury might result in osteoblast proliferation. iOcn mice were crossed with *Rosa26-loxP-stop-loxP-DTR* (iDTR, inducible diphtheria toxin receptor) mice. In *Ocn-Cre-ER*$^+$ *Rosa-YFP*$^+$ *iDTR*$^+$ trigenic mice (hereafter iOcn/iDTR), the administration of 4-OHT can induce both YFP and DTR expression specifically within mature osteoblasts. Injecting low-dose diphtheria toxin (DT) and tracking Ocn/YFP^+ osteoblasts, we noted ~90% elimination of the labeled cells at 7 days (Figure 1G, right). Control DT-treated iOcn mice without DTR showed no effect on labeled osteoblasts (data not shown). The remaining Ocn/YFP^+ osteoblasts were evaluated intermittently over a 3 month interval and no increase or clustering of Ocn/YFP^+ osteoblasts was noted (Figure 1G), further demonstrating that mature osteoblasts do not proliferate.

Osterix$^+$ Osteolineage Cells Are a Transient Source of Osteoblasts in Adult Mice

O*sterix* (*Osx*) is known to be expressed earlier than *osteocalcin* in the osteoblast lineage (Rodda and McMahon, 2006). A recent report showed that osterix-expressing preosteoblasts are the origin of trabecular osteoblasts and osteocytes in developing bones (Maes et al., 2010). A similar relationship between cells was observed in fracture healing (Maes et al., 2010). This population is also thought to be important in regulating hematopoiesis (Raaijmakers et al., 2010; Walkley et al., 2007a). We therefore examined the expansion and durability of YFP$^+$ cells using a mouse where the *Osx* promoter drives a Cre-ER fusion gene, crossed with *Rosa-YFP* reporter mice to generate *Osx-Cre-ER*$^+$ *Rosa-YFP*$^+$ (herein iOsx) mice (Figures 2A and S2A). To test whether preosteoblasts contribute to the long-term maintenance of mature osteoblasts under homeostasis, we conducted genetic pulse-chase experiments using iOsx reporter mice. Fourteen days after 4-OHT treatment, intravital microscopy analysis and anti-GFP/YFP immunohistochemistry revealed that, unlike Ocn/YFP$^+$ mature osteoblasts, most Osx/YFP$^+$ preosteoblasts were detected in the outer margin and the osteogenic front of sutures or bone marrow. Only a small portion of cells (<20%) were located on the endosteal surface of marrow cavities (Figures 2A and S2B). Therefore, we selected a specific region covering the first frontal bone cavity and the S.S., located in the left side of the S.S. and C.S. intersection, and counted the number of Osx/YFP$^+$ preosteoblasts and their progeny. Tracing of labeled preosteoblasts by sequential imaging revealed that the average number of Osx/YFP$^+$ cells increased temporarily at 30 days after induction, but later decreased, and returned to the basal level at ~90 days (Figures 2B and 2C). We confirmed this with anti-GFP/YFP immunohistochemistry on femoral bone, and their differentiation, with anti-Ocn immunohistochemistry (Figures S2C and S2D). Consistent with a previous study (Maes et al., 2010), we observed that distinct Osx/YFP$^+$ cells on the periosteal surface near the suture were Ki-67$^+$ (Figure 2D). However, the percentage of Ki-67$^+$ cells within *Osx*-labeled cells from adult bones was much lower (~1%; 2–3 cells/200 counted, n = 3) than that from developing bones (22% ± 3%) (Maes et al., 2010) and, like the *Ocn*-labeled cells, there was no durable labeling of *Osx*-labeled preosteoblasts. This result suggests that the osterix-expressing population does not represent a self-renewing pool of progenitors.

To confirm that the labeled mature osteoblasts were continuously replaced by new osteoblasts, iOcn mice imaged at day 60 after the first 4-OHT treatment were followed for 2 additional months and a second sequence of 4-OHT was administered. At 14 days after the second 4-OHT pulse, imaging the same sites revealed an increase in the number of Ocn/YFP$^+$ osteoblasts (Figure 2E). This increase was approximately equivalent to the number observed at 14 days after the first 4-OHT treatment, and the numbers again decreased with similar kinetics (data not shown).

Taken together, these data demonstrate that existing osteoblasts and preosteoblasts turn over rapidly and are continuously replaced by new osteoblasts. If the new osteoblasts were derived from division of the existing osteoblasts, genetically labeled 2–3 three months earlier, we would have anticipated that the portion of labeled cells would remain relatively constant over this period. Because labeling of osteoblasts instead required a second activation of Cre recombinase, the new cells were likely derived from a different cell source that had not previously expressed the osteoblast markers *Ocn* and *Osx*.

Long-Term Maintenance of Osteogenic Cells Is Provided by Progenitors

The *myxovirus resistance-1* (*Mx1*) promoter has been shown to be activated in bone marrow stromal cells of undefined identity (Walkley et al., 2007b). In an attempt to define a marker for more immature osteolineage cells, we assessed *Mx1-Cre* mice crossed with *Rosa-YFP* reporter mice (hereafter Mx1/YFP). Twenty days after pIpC administration (25 mg/kg every

other day for 10 days) to activate *Mx1*, we observed YFP labeling in 70% ± 8% of endosteal bone cells (Figures 3A [top] and 3C). Additional immunohistochemistry with anti-Ocn, anti-osteopontin (expressed by mature osteoblasts; data not shown), and anti-Osx antibodies confirmed that the Mx1/YFP$^+$ cells on the endosteal surface of bones were osteogenic cells (Figure 3A, top middle and right). Because *Mx1*-inducible cells include hematopoietic-derived osteoclasts (Walkley et al., 2007b), it is possible that some of YFP$^+$ bone cells were osteoclasts. To exclude this possibility and improve specific cell quantification, we developed trigenic *Mx1-Cre*$^+$ *Rosa-Tomato*$^+$ *Ocn-GFP*$^+$ mice (Mx1/Tomato/Ocn-GFP) by crossing *Mx1-Cre* mice with *Rosa26-loxP-stop-loxP-tdTomato* reporter and *Ocn-GFP* mice, allowing the distinction between *Mx1*-induced osteoblasts (red and green) and *Mx1* noninducible osteoblasts (green). Flow cytometric analysis showed that 88% of Ocn$^+$ osteoblasts were red and green at 30 days postinduction (Figure 3B), confirming that *Mx1* labels the majority of endosteal bone cells. Next, to examine the durable labeling of *Mx1* and to eliminate *Mx1*-inducible hematopoietic cells, we transplanted wild-type marrow cells (WT-BMT) into lethally irradiated Mx1/YFP mice and, 8 weeks later, induced *Mx1* activity by pIpC treatment. Over 6–10 months after labeling (four to five cycles of osteoblast turnover), about 80% of Ocn$^+$ osteoblasts on the endosteal surface in femurs and calvaria remained YFP$^+$ (Figures 3A [bottom], 3C, and S3B), indicating that the labeling of osteoblasts by *Mx1* is durable. We observed similar results in nonirradiated, non-WT-BMT animals (Figure S3A). We confirmed low basal activity of *Mx1-Cre* and the specificity of these data by anti-GFP/YFP and ant-Ocn immunohistochemistry with femurs from the indicated control mice (Figures 3C [−pIpC] and S3C). The level of *Mx1*-induced hematopoietic cells was less than 1% (6 months) or undetectable (10 months) in the mice (data not shown), arguing against a contribution of *Mx1*-induced osteoclasts to the endosteal cell population. Comparing osteoblast labeling with that of the hematopoietic compartment revealed that the percentage of marked osteolineage cells was similar to the labeling of LT-HSCs (Kiel et al., 2005) (>95%, Figures S3C and S3D), but much higher than that of mature hematopoietic cells (~40%–60%, Figures S3E and S3F), further suggesting that *Mx1-Cre* can efficiently label osteogenic stem/progenitors.

Previously, it has been suggested that mesenchymal/osteogenic progenitors are located in midsuture and are critical for calvarial bone growth, whereas more differentiated osteogenic cells are in the osteogenic fronts of parietal bones (Lana-Elola et al., 2007). Consistent with this, most of the midsuture mesenchymal cells from all sutures examined in Mx1/YFP mice were homogeneously and durably labeled by the *Mx1* promoter, whereas GFP$^+$ cells labeled by activity of the *Col2.3* (an osteoblastic promoter induced by *Osx*) and *Ocn* promoters were detected only in the osteogenic fronts of the parietal bones (Figure S3G). In addition, flow cytometric analysis of CD45$^-$CD105$^+$ osteogenic progenitor fraction (Chan et al., 2009) showed constant labeling at 40 days after induction (Figure S3C), indicating that the induction of *Mx1* labels endogenous osteogenic stem/progenitors that can maintain the majority (>80%) of mature osteoblasts over time in the adult mouse.

Mx1-Induced Progenitors Are Clonogenic and Have Multilineage Differentiation Potential In Vitro

Others have demonstrated that mesenchymal stem/progenitor cells are enriched in the Sca1$^+$CD90$^+$ or Sca1$^+$CD140a$^+$ bone marrow fractions (Chan et al., 2009; Morikawa et al., 2009). We found that 93% of clonogenic stromal cells were present in the nonhematopoietic (CD45$^-$Ter119$^-$CD31$^-$) CD105$^+$CD140a$^+$ bone cells (5.4% ± 2.9%, Figure 3D). Further immunophenotypic analysis revealed that this fraction was similar to the recently defined Sca1$^+$CD140a$^+$ MSCs, with uniformly high expression of Sca-1, CD29, CD44, and CD133 and lower expression of CD90, CD49d, and CD71 (Morikawa et al., 2009) (Figure S3H). To test whether *Mx1-Cre* marks this fraction, analysis of Mx1/YFP mice revealed that 44% ±

9% of the $CD105^+CD140a^+$ fraction was YFP^+ and the fraction marked with YFP was enriched for ~80% of the clonogenic cells. The clonogenic frequency of this fraction is ~1 in 20, which is 50-fold higher than that of $CD45^-Ter119^-$ cells (~1/1,000) and ~50,000 fold higher than that of unfractionated bone marrow stromal cells (~$1/1 \times 10^6$ cells) (Figure 3E). Those colonies that emerged from the YFP^- fraction were morphologically distinct, resembling what others have described as endothelial cells (Morikawa et al., 2009). Using a single pulse of pIpC and in vivo imaging, we defined that *Mx1* labels a majority of osteogenic progenitors and a fraction of Ocn^+ mature osteoblasts (Figure S4A), but not osteocytes (data not shown). However, GFP^+ cells from *iOcn, iOsx*, or *Col2.3-GFP* mice comprised <3% of the $CD105^+CD140a^+$ fraction and did not form colonies (Figures S4B and S4C). Therefore, *Mx1* induction labels an immature, clonogenic subset of the CD105- and CD140a-expressing putative MSCs, and by comparison with the results of labeling more mature populations, it can be used to discern MSC function in vivo.

When *Mx1*-induced progenitors ($YFP^+CD105^+CD140a^+$ $CD45^-Ter119^-CD31^-$) were single-cell sorted and cultured, single *Mx1*-induced progenitors formed colonies that were YFP^+ (Figure S4D). Cells from a single, dispersed and split $Mx1/YFP^+$ colony were cultured under differentiation conditions and demonstrated the ability to become osteoblasts, adipocytes, and chondrocytes at a single-cell level in vitro (Figure 3F). These analyses indicate that *Mx1*-labeled colony-forming cells are consistent with what others have called MSCs at a single-cell level by in vitro analysis.

One limitation of our single reporter system is that the possible existence of $Mx1^-$ MSCs or the increase of their descendents would not be visualized. To overcome this limitation, we crossed *Mx1-Cre* mice with *Rosa26-loxP-mTomato-loxP-mEGFP* (mTmG) dual reporter mice (hereafter Mx1/mTmG). In this model, the mTomato cassette is deleted in the *Mx1-Cre* inducible cells, allowing the expression of the GFP, while *Mx1* noninducible cells and their progeny express mTomato and remain red. After wild-type marrow transplantation followed by pIpC treatment and an additional 90 days of incubation, anti-Ocn immunohistochemical analysis of femurs showed that the vast majority (>90%) of osteoblasts on the endosteal surface and of suture mesenchymal cells maintained GFP labeling homogenously (Figures 3G [top] and S3G [right]). The persistence of Mx1/GFP labeling and absence of dilution by unlabeled cells suggests that *Mx1* efficiently labels osteolineage cells and that more immature $Mx1^-$ (red) progenitors did not contribute significantly to osteoblastic homeostasis. A known marker of a rare quiescent MSC population capable of multilineage cell production is the cytoskeletal component nestin (Méndez-Ferrer et al., 2010). We found that most (~59%), but not all, $nestin^+$ cells in the bone marrow were also Mx1/GFP labeled (Figure 3G, bottom). Using a nestin-GFP mouse, we confirmed that $nestin^+$ cells are highly enriched in the $CD105^+140a^+$ fraction (43%) and that nestin is also highly expressed in suture mesenchymal cells (Figures S4E and S4F), similar with Mx1/YFP mouse. Therefore, $Mx1/GFP^+$ cells overlap with at least a subpopulation of the $nestin^+$ MSCs in the bone marrow.

Limited Lineage Potential of *Mx1*-Induced MSCs In Vivo

Because *Mx1*-induced progenitors met the ex vivo criteria for MSCs, we used these cells to test the potential for such cells to exert their putative multipotency in vivo. The staining of chondrocytes in femurs from Mx1/YFP mice (+pIpC at 6–8 weeks age) by anti-aggrecan antibody revealed no YFP signal in chondrocytes in either articular cartilage or the growth plate (data not shown) at 40 days, 6 months, (Figure 4A), or up to 10 months (Figure S3B, middle) after pIpC induction. Even when *Mx1* activity was induced when bone and cartilage development was active (P7), no YFP signal was apparent in chondrocytes (Figure 4A, +pIpC at P7), indicating an absence of in vivo chondrogenic potential.

To assess adipocyte potential of *Mx1*-induced progenitors, we examined bone marrow and periosteal adipocytes at varying ages. Despite a more than 10-fold increase of bone marrow adipocytes as measured by anti-perilipin antibody staining in old *Mx1*-induced mice (12 months old with 6 months after pIpC following 2 months after BMT) as compared with young *Mx1*-induced mice (4 months old with 40 days after pIpC), neither population of mice had >5% of adipocytes marked by *Mx1-Cre* (Figures 4B, S5A, and S5B). These data suggest that adipogenic differentiation of *Mx1*-induced progenitors in adult mice is rare despite the generation of new adipocytes in the bone marrow and the adipogenic capacity of the cells ex vivo.

To further confirm these data, we employed Mx1/mTmG dual reporter mice, which are described in Figure 3G. Consistent with the Mx1/YFP model, in vivo imaging of calvaria showed that the vast majority of osteoblasts on the endosteal surface and of suture mesenchymal cells maintained mGFP labeling homogenously (Figure 4D, left). Interestingly, many perivascular cells close to the endosteal surface were labeled with GFP, a site reported by others to be the location of MSCs (Figures 4C and S5C) (Méndez-Ferrer et al., 2010). In addition, immunohistochemical analysis of femurs showed that all chondrocytes, skeletal muscle cells, fibroblasts, and blood vessels remained red, supporting the idea that they are functional, but *Mx1* noninducible (Figures 4D, S5D, and S5E). Therefore, *Mx1* induction labels MSC-like cells in vivo that are only fated to the osteolineage, and not these other cell types, under physiological conditions in the adult mouse skeleton.

Mx1-Induced Osteogenic Stem/Progenitors Are the Source of New Osteoblasts for Fracture Repair In Vivo

Fracture healing is associated with an increase in local osteoblasts (Leucht et al., 2007). However, the origin of new osteoblasts in fracture sites has not been clearly demonstrated (Schindeler et al., 2008). Therefore, to define the source of the osteoblasts located at injury sites, we generated microfractures of the calvarium using needle wounding at osteostage-specific pulse-labeled animals. When Ocn/YFP$^+$ mature osteoblasts (iOcn mice) and Osx/YFP$^+$ preosteoblasts (iOsx mice) were tracked for 7 days after injury, they increased in number at the injury site, but only small numbers were detected by sequential in vivo imaging (Figures 5A [top] and 5B). In contrast, *Mx1*-induced osteogenic cells in Mx1/mTmG mice newly appeared in the site of the fracture at 2 days and dramatically increased at 7 days after injury (Figures 5A [bottom] and S6A). Most of the osteogenic cells at the fracture site were GFP$^+$ and the number of *Mx1*-induced cells at the injury site increased by more than 100- fold (Figure 5B, square). By anti-Ki-67 immunohistochemistry, no anti-Ki-67 staining in iOcn mice and rare staining (<3%) in iOsx mice was evident (Figure S6B). However, >10% of *Mx1*-induced osteogenic cells were Ki-67$^+$ in Mx1/mTmG mice (Figure 5C, top). This fraction was much higher than that in uninjured bones (<1%; data not shown) and new clusters of Mx1/GFP$^+$ osteogenic cells observed at the fracture site stained positively for Ocn (Figure 5C, bottom), indicating the responsiveness of this population to physiologic challenge. Of note, these cells did not stain with anti-CD45 and were therefore not inflammatory cells that had consumed the GFP dye (Figure S6C). To further distinguish and enumerate stem/progenitor cells and mature osteoblasts during fracture healing, we used trigenic Mx1/Tomato/Ocn-GFP dual reporter mice. In this model, *Mx1*- induced stem/progenitors express Tomato and their osteoblastic progeny express Tomato and GFP, while mature osteoblasts from *Mx1*-noninducible progenitors express GFP alone. When mature osteoblasts and their progenitors were tracked for 21 days after injury, *Mx1*-induced stem/progenitors (Tomato$^+$) newly appeared in the site of the fracture at 2–5 days and dramatically increased in number at 12 days. Subsequently, *Mx1*-labeled stem/progenitors near the fracture surface differentiated into GFP$^+$ osteoblasts (Figure 5D, day 12, yellow).

More importantly, most osteoblasts associated with new bone (analyzed by second harmonic generation; blue) at the fracture site were Tomato and GFP double positive, and there were no observable GFP single positive osteoblasts. These results demonstrate that the migration and proliferation of osteogenic progenitor cells labeled by *Mx1* supply the majority of osteoblastic cells participating in fracture healing (Figure 5D, day 21). Consistently, when microfractures were generated at distal metaphysis and articular cartilage of femoral bones, the number of *Mx1*-labeled periosteal (inner cambial) and endosteal osteoblasts at the fracture site markedly increased compared to that in uninjured bones at 21 days after injury (Figure 5E). In addition, newly generated chondrocytes during the fracture healing remained $Mx1^{-}$ (Figure 5E, right, white arrows), further supporting the idea that the *Mx1*-labeled osteogenic stem/progenitors (OSPCs) are distinct from chondrogenic progenitors.

To test the migration of osteoblasts toward injury in vivo, continuous Z-stack imaging of individual cells with intravital microscopy was conducted over 7 hr at 24 hr after injury (Figure S6D). In addition, we sequentially scanned the detailed structures of bone matrix, osteoblasts, and vessels near the injury sites immediately (0 hr), 24 hr, and 48 hr after injury (Figure 5F). We noted that multiple Ocn/YFP^{+} osteoblasts appeared to move toward the injury site. We confirmed these results by Z-stack imaging (Figure S6E). Interestingly, the endosteal Ocn/YFP^{+} osteoblasts of the uninjured controls were also observed to shift position in a manner not explained by the subject's breathing or pulse (data not shown).

Transplantation Capability of OSPCs

We next tested whether osteogenic stem/progenitors isolated from Mx1/YFP mice were capable of translocating by a blood-borne route. *Mx1*-induced OSPCs (isolated as in Figure 3E, red box) from these mice transplanted with wild-type marrow were isolated by flow cytometry and injected intravenously into nonirradiated (Figures 6A [left] and S7A) or sublethally irradiated (Figures 6A [right] and S7B) wild-type recipients. The Mx1/YFP^{+} OSPCs homed to the abluminal surface of sinusoidal vessels in the bone marrow at day 7, increased in number, and stably incorporated as bone units on endosteal surfaces for at least 4 months with over 70% (5/7) engraftment efficiency. They further differentiated into Ocn^{+} mature osteoblasts at multiple sites in femurs (Figure 6B). In contrast, transplantation of control $YFP^{+}CD105^{+}CD140a^{-}$ cells (isolated as in Figure 3D, box A) from *Mx1*-induced mice (data not shown) or GFP^{+} cells (mature osteoblasts) from *Col 2.3kb*-GFP mice did not reveal YFP^{+} or GFP^{+} cells on the endosteal surface (Figure 6A, top). We compared the homing of OSPCs with that of HSPCs ($LKSCD48^{-}CD150^{+}$) (Kiel et al., 2005) by in vivo imaging of calvarial bone marrow cavities (Lo Celso et al., 2009) and found that OSPCs homed to bone marrow with an efficiency of ~15%–20% that of HSCs (Figure 6C). Therefore, *Mx1*-induced OSPCs can translocate by vascular spread and engraft at distal sites.

Functional Capacity of Transplanted *Mx1*-Induced OSPCs

Although we observed long-term engraftment and osteoblast differentiation of transplanted *Mx1*-induced OSPCs, their functional contribution to recipient bones was not clear. Therefore, we assessed the in vivo contribution of transplanted OSPCs in the repair of fractured bone in aged female animals as an assessment of potential in a model resembling a clinical need. Using the same number of freshly isolated mature osteoblasts (*Col2.3kb*-GFP-labeled) or OSPCs (*Mx1*-labeled) in matrigel, we transplanted cells at the site of mechanical injury and examined bone repair. We observed engraftment of OSPCs in substantially increased numbers at the fracture sites (Figure 7A). These cells differentiated into functional osteoblasts (Ob) and osteocalcin-expressing osteocytes (Ocy) (Figure 7B, right) producing a bone bridge and ectopic mineralized bones (Figures 7A [arrows] and 7B [black squares]) in marked contrast to transplanted mature osteoblasts (Figure 7A, top). We confirmed these

results by anti-type-I collagen immunohistochemistry (data not shown). Next, to further test their progenitor function, we assessed the clonal dynamics of *Mx1*-labeled OSPCs. When single *Mx1*-labeled OSPCs were isolated, transplanted, and tracked in vivo, they rapidly generated new progenitors at the site of injury (Figure 7C, day 7). Later, these cells acquired features of differentiated osteoblasts (red and green) and produced mineralized bone (blue) (Figure 7C, day 21), while some of them remained as progenitors (red). These data indicate that *Mx1*-induced OSPCs can be transplanted and functionally contribute to the recovery of injured bones. When transplanted at a limiting dilution level, OSPCs rapidly generated new cells with ~1 in 40 engraftment efficiency in vivo at the site of injury (Figure 7D). When *Mx1*-labeled cells were reisolated at 4 weeks after transplantation, 33% ± 5% preserved progenitor characteristics and successfully repopulated with secondary transplantation (Figure 7E). These data indicate that *Mx1*-induced OSPCs can be transplanted, and that they functionally contribute to the recovery of injured bones. Further, the stem/progenitor cells are capable of secondary transplantation, indicating that they can either self-renew or at least be maintained at the injury site.

DISCUSSION

The studies presented here clarify the source and lifespan of osteoblasts in the adult mouse, building on historic work using morphologic definitions of cells and ^{3}H-thymidine incorporation in a mixed cell population (Jilka et al., 1998; McCulloch and Heersche, 1988; Owen and MacPherson, 1963). The use of genetic tools now permits a more precise definition of the short lifespan (~60 days) and postmitotic state of mature osteoblasts, the duration and modest proliferation of preosteoblasts, and the self-preserving nature and rapid cell cycling of the osteogenic stem/progenitor cells that maintain life-long osteolineage cells.

The identity and in vivo multipotency of putative MSCs from various different tissues has been a source of controversy (Caplan and Correa, 2011). The MSC as most commonly defined is a cell with CFU-F and multilineage differentiation potential in vitro. Our data indicate that *Mx1*-induced cells satisfy the characteristics of what has been termed an MSC by immunophenotype, clonogenic capacity, single cell-derived multilineage differentiation capability ex vivo, and in vivo osteogenic differentiation and new bone formation after transplantation. These bone marrow cells appear to be a subset of the generally quiescent nestin^{+} cells that contribute to the HSC niche (Méndez-Ferrer et al., 2010) and may not reflect all of the different cell populations that have been termed “MSCs” and studied by others. The *Mx1*-induced cells are predominantly osteolineage restricted with only a minimal amount of adipocytic cell marking with lineage tracing and are more consistent with a skeletal stem cell as proposed by Bianco et al. than a broadly defined MSC (Bianco et al., 2008). Whether the adipocytes derived in vivo from bipotential *Mx1*-induced cells or a distinct subset within the *Mx1*-induced pool cannot be determined. However, our data clearly demonstrate that *Mx1*-induced cells do not label chondrocytes both under homeostatic and after fracture injury in vivo, a population that has been shown to be a descendent of nestin-labeled cells (Méndez-Ferrer et al., 2010). These data imply that *Mx1*-induced OSPCs do represent a distinct and not entirely overlapping subset of nestin^{+} cells, suggesting the possible heterogeneity of nestin^{+} cells in bone marrow with distinct lineage capability.

The bone healing mechanism and the source of new osteoblasts in fracture sites have been long controversial (Schindeler et al., 2008). *Mx1*-induced OSPCs are responsive to stress conditions and fracture in contrast to *Osx*-labeled or *Ocn*-labeled osteoblasts. By the sequential imaging of fracture sites in *Mx1* and *Ocn* dual reporter mice, osteogenic progenitors were shown to appear at the site of injury as early as 2 days after injury and proliferate, with the cells close to the fracture differentiating into functional osteoblasts. In

addition, the absence of distinct osteoblasts that failed to label with *Mx1* within the injury indicates that *Mx1*-labeled OSPCs are the source of new osteoblasts during fracture healing (Figure 5D). Although we did not test whether OSPCs circulate under physiologic conditions, as reported by others (Otsuru et al., 2008), we observed that they are capable of translocating locally and via the vasculature by transplantation. Taken together, our data demonstrate that the contribution of this subset of putatively multipotent BMSCs to bone regeneration and repair is very lineage limited in adult animals in vivo and that *Mx1* labels an osteolineage stem/progenitor population.

The ability of proliferating, durable stem/progenitor cells to replace short-lived mature cells and to translocate to local and distant sites poses an interesting possibility for their involvement in disease. The prior studies indicate that altered marrow micro-environmental cells can induce hematopoietic disease (Raaijmakers et al., 2010; Walkley et al., 2007a), giving them a greater potential as a disease mechanism based on the findings here. Inherited genetic syndromes (such as Schwachmann-Diamond Syndrome) are plausibly associated with a broad-based defect in hematopoietic support on the basis of skeletal defects as suggested by prior studies deleting the disease-associated gene (*Sbds*) selectively in preosteoblasts (Raaijmakers et al., 2010). Contributions to acquired disease would be in question if mature cells turned over rarely and were replaced by mature cell division. If mature cells turn over rapidly and are replaced by an amplifying pool of stem/progenitors, the likelihood that acquired genetic lesions in that primitive pool could persist, accumulate, and yield large numbers of mature cells increases. The genetic pulse-chase studies of endogenous osteolineage stem/progenitors presented here provide data that such a population exists in vivo, is replicative, and is responsible for dynamically replacing the short-lived osteolineage in homeostasis or after injury. Further, these cells can translocate, indicating their potential to have a more systemic effect than would be expected from a highly locally constrained pool. Together, our studies indicate that mesenchymal cells in bone and bone marrow have a hierarchical organization of long-term repopulating progenitors serving to replace short-lived, postmitotic, mature cells, similar to tissues such as the blood, skin, and intestine.

To be clear, we point out that the cells we have studied here are a subset of mesenchymal cells in the bone marrow. They may not reflect the behavior of putative MSCs from other tissues or other bone marrow subsets of mesenchymal cells. There may indeed by true multipotent mesenchymal stem cells (such as some of the nestin-expressing cells). However, our data indicate that multipotentcy ex vivo should be regarded with caution, as it is not a reliable guide as to how the cells will function in vivo. The $Mx1^{+}$ subset of BMSCs is, in vivo, an osteolineage-restricted stem/progenitor cell subset.

EXPERIMENTAL PROCEDURES

Mice

Six- to eight-week-old C57BL/6 mice, *Mx1-Cre* (B6.Cg-Tg(Mx1-cre)1Cgn/J), *Rosa26-loxP-stop-loxP-EYFP* (Rosa-YFP, B6.129X1-*Gt(ROSA)26Sor*$^{tm1(EYFP)Cos}$/J), *Rosa26-loxP-stop-loxP-tdTomato* (Rosa-Tomato, B6.Cg-*Gt(ROSA)26Sor*$^{tm9(CAG-tdTomato)Hze}$/J), *Rosa26-loxP-stop-loxP-DTR* (iDTR) (Buch et al., 2005), and *Rosa26-loxP-mTomato-loxP-mEGFP* (mTmG, B6.129(Cg)-*Gt(ROSA)26Sor*$^{tm4(ACTB-tdTomato–EGFP)Luo}$/J) were purchased from Jackson laboratory. *Col2.3-GFP, Ocn-GFP, Osx-Cre-ER* (Maes et al., 2010) and *Ocn-Cre-ER* (C57BL/6 background) mice were provided by author H.M.K. The induction of iDTR and *Mx1* is described in Supplemental Experimental Procedures. All mice were maintained in pathogen-free conditions, and all procedures were approved by Institutional Animal Care and Use Committee (IACUC).

In Vivo Imaging

To image YFP^+ osteoblasts and osteogenic progenitors in vivo, indicated mice were anesthetized and prepared for a custom-built two-photon and confocal hybrid microscope specifically designed for live animal imaging as described previously (Sipkins et al., 2005) (Lo Celso et al., 2009). Briefly, to trace the change in osteoblast number over time, the injured site or the first frontal bone cavity located in the upper left side of the S.S. and C.S. intersection was mapped by four to six consecutive images (660 μm^2/image), which covered most of the endosteal osteoblasts (YFP), the vessel network (Q-dots), and the bone structures (second harmonic generation by multiphoton laser) in the cavity. Each image was recorded by Z-stacks with 50–100 μm depth from bone surface and 2 μm interval. Details in intravital microscopy are described in Supplemental Experimental Procedures. 3D images were reconstructed using Nikon NIS-Elements software, and osteoblast numbers were counted. A two-tailed type 2 t test was applied to all data. $p < 0.05$ was considered statistically significant.

Creation of Microfractures and Live Animal Imaging after Injury

For live imaging of osteoblasts near injury, a small incision was introduced on the scalp of indicated mice, and two separate microfractures were generated by a 25G or a 27G needle drilling on the surface of calvaria near the intersection of the S.S. and C.S. Ocn/YFP^+, Osx/YFP^+, Mx1/YFP^+, or Mx1/Tomato cells near the injury were tracked by sequential in vivo imaging at the indicated time points. Separately, a small incision was introduced on the right knee and two separate microfractures were generated by needle drilling (20G) at distal metaphysis and articular cartilage of femurs of wild-type marrow-transplanted and pIpC-treated *Mx1* reporter mice. Three weeks after injury, injured and uninjured (control) femurs were analyzed by immunofluorescence staining using the indicated antibodies and hematoxylin and eosin (H&E) staining.

In Vivo Imaging of Transplantated Osteogenic Stem/Progenitors

Mx1/YFP^+ OSPCs ($CD45^-Ter119^-CD31^-CD105^+CD140a^+YFP^+$) from lethally irradiated Mx1/YFP mice or GFP^+ cells from *Col2.3-GFP* mice were FACS sorted. The sorted cells (5,000 cells/mouse) in 200 μl of PBS were transplanted intravenously into wild-type mice, or the indicated number of sorted cells mixed with 20 μl of matrigel (BD Biosciences) were transplanted upon calvarial injury of normal (for limiting dilution assay) or ~1-year-old wild-type female mice (for ectopic bone formation). To measure in vivo homing ability of osteogenic stem/progenitors, 1,000 sorted $Mx1^+$ OSPCs and 1,000 sorted HSCs (DiD-stained) were mixed and transplanted into irradiated mice. The implantation of donor cells at the sites of injury was analyzed by in vivo imaging and immunofluorescence staining.

Isolation and Flow Cytometry Analysis of Osteoprogenitor Cells

Isolation of osteoprogenitors from compact bones was done by following mouse mesenchymal progenitor isolation protocols from STEMCELL technologies. Details are described in the Supplemental Experimental Procedures.

CFU-F, Ex Vivo Multilineage Differentiation, and Immunofluorescence

Details are described in the Supplemental Experimental Procedures.

Supplementary Material

Refer to Web version on PubMed Central for supplementary material.

Acknowledgments

We thank C. Lo Celso, S. Mukherjee, J. Schoonmaker, S. Guo, R. Schlanger, and M. Kim for advice and technical assistance; N. Jeanson, A. Catic, J. Dietrich, and D. Sykes for reading the manuscript; the HSCI/MGH CRM Flow Core (L. Prickett, K. Folz-Donahue, and D. Dombkowski); and the Leukemia & Lymphoma Society (Fellowship Award to D.P.) and the National Institutes of Health (grants to T.L.C., C.P.L., H.M.K., and D.T.S.).

REFERENCES

Bianco P, Robey PG, Simmons PJ. Mesenchymal stem cells: revisiting history, concepts, and assays. Cell Stem Cell. 2008; 2:313–319. [PubMed: 18397751]

Buch T, Heppner FL, Tertilt C, Heinen TJ, Kremer M, Wunderlich FT, Jung S, Waisman A. A Cre-inducible diphtheria toxin receptor mediates cell lineage ablation after toxin administration. Nat. Methods. 2005; 2:419–426. [PubMed: 15908920]

Caplan AI. Mesenchymal stem cells. J. Orthop. Res. 1991; 9:641–650. [PubMed: 1870029]

Caplan AI, Correa D. The MSC: An Injury Drugstore. Cell Stem Cell. 2011; 9:11–15. [PubMed: 21726829]

Chan CK, Chen CC, Luppen CA, Kim JB, DeBoer AT, Wei K, Helms JA, Kuo CJ, Kraft DL, Weissman IL. Endochondral ossification is required for haematopoietic stem-cell niche formation. Nature. 2009; 457:490–494. [PubMed: 19078959]

Crisan M, Yap S, Casteilla L, Chen CW, Corselli M, Park TS, Andriolo G, Sun B, Zheng B, Zhang L, et al. A perivascular origin for mesenchymal stem cells in multiple human organs. Cell Stem Cell. 2008; 3:301–313. [PubMed: 18786417]

Dallas SL, Bonewald LF. Dynamics of the transition from osteoblast to osteocyte. Ann. N Y Acad. Sci. 2010; 1192:437–443. [PubMed: 20392270]

Dominici M, Rasini V, Bussolari R, Chen X, Hofmann TJ, Spano C, Bernabei D, Veronesi E, Bertoni F, Paolucci P, et al. Restoration and reversible expansion of the osteoblastic hematopoietic stem cell niche after marrow radioablation. Blood. 2009; 114:2333–2343. [PubMed: 19433859]

Dor Y, Brown J, Martinez OI, Melton DA. Adult pancreatic beta-cells are formed by self-duplication rather than stem-cell differentiation. Nature. 2004; 429:41–46. [PubMed: 15129273]

Ducy P, Desbois C, Boyce B, Pinero G, Story B, Dunstan C, Smith E, Bonadio J, Goldstein S, Gundberg C, et al. Increased bone formation in osteocalcin-deficient mice. Nature. 1996; 382:448–452. [PubMed: 8684484]

Eghbali-Fatourechi GZ, Lamsam J, Fraser D, Nagel D, Riggs BL, Khosla S. Circulating osteoblast-lineage cells in humans. N. Engl. J. Med. 2005; 352:1959–1966. [PubMed: 15888696]

Friedenstein AJ, Chailakhyan RK, Latsinik NV, Panasyuk AF, Keiliss-Borok IV. Stromal cells responsible for transferring the microenvironment of the hemopoietic tissues. Cloning in vitro and retransplantation in vivo. Transplantation. 1974; 17:331–340. [PubMed: 4150881]

Jilka RL, Weinstein RS, Bellido T, Parfitt AM, Manolagas SC. Osteoblast programmed cell death (apoptosis): modulation by growth factors and cytokines. J. Bone Miner. Res. 1998; 13:793–802. [PubMed: 9610743]

Kalajzic Z, Li H, Wang LP, Jiang X, Lamothe K, Adams DJ, Aguila HL, Rowe DW, Kalajzic I. Use of an alpha-smooth muscle actin GFP reporter to identify an osteoprogenitor population. Bone. 2008; 43:501–510. [PubMed: 18571490]

Kiel MJ, Yilmaz OH, Iwashita T, Yilmaz OH, Terhorst C, Morrison SJ. SLAM family receptors distinguish hematopoietic stem and progenitor cells and reveal endothelial niches for stem cells. Cell. 2005; 121:1109–1121. [PubMed: 15989959]

Lana-Elola E, Rice R, Grigoriadis AE, Rice DP. Cell fate specification during calvarial bone and suture development. Dev. Biol. 2007; 311:335–346. [PubMed: 17931618]

Lee NK, Sowa H, Hinoi E, Ferron M, Ahn JD, Confavreux C, Dacquin R, Mee PJ, McKee MD, Jung DY, et al. Endocrine regulation of energy metabolism by the skeleton. Cell. 2007; 130:456–469. [PubMed: 17693256]

Leucht P, Kim JB, Wazen R, Currey JA, Nanci A, Brunski JB, Helms JA. Effect of mechanical stimuli on skeletal regeneration around implants. Bone. 2007; 40:919–930. [PubMed: 17175211]

Li L, Clevers H. Coexistence of quiescent and active adult stem cells in mammals. Science. 2010; 327:542–545. [PubMed: 20110496]

Lo Celso C, Fleming HE, Wu JW, Zhao CX, Miake-Lye S, Fujisaki J, CÔté D, Rowe DW, Lin CP, Scadden DT. Live-animal tracking of individual haematopoietic stem/progenitor cells in their niche. Nature. 2009; 457:92–96. [PubMed: 19052546]

Maes C, Kobayashi T, Selig MK, Torrekens S, Roth SI, Mackem S, Carmeliet G, Kronenberg HM. Osteoblast precursors, but not mature osteoblasts, move into developing and fractured bones along with invading blood vessels. Dev. Cell. 2010; 19:329–344. [PubMed: 20708594]

McCulloch CA, Heersche JN. Lifetime of the osteoblast in mouse periodontium. Anat. Rec. 1988; 222:128–135. [PubMed: 3213963]

Méndez-Ferrer S, Michurina TV, Ferraro F, Mazloom AR, Macarthur BD, Lira SA, Scadden DT, Ma'ayan A, Enikolopov GN, Frenette PS. Mesenchymal and haematopoietic stem cells form a unique bone marrow niche. Nature. 2010; 466:829–834. [PubMed: 20703299]

Morikawa S, Mabuchi Y, Kubota Y, Nagai Y, Niibe K, Hiratsu E, Suzuki S, Miyauchi-Hara C, Nagoshi N, Sunabori T, et al. Prospective identification, isolation, and systemic transplantation of multipotent mesenchymal stem cells in murine bone marrow. J. Exp. Med. 2009; 206:2483–2496. [PubMed: 19841085]

Otsuru S, Tamai K, Yamazaki T, Yoshikawa H, Kaneda Y. Circulating bone marrow-derived osteoblast progenitor cells are recruited to the bone-forming site by the CXCR4/stromal cell-derived factor-1 pathway. Stem Cells. 2008; 26:223–234. [PubMed: 17932420]

Owen M, MacPherson S. Cell Population Kinetics of an Osteogenic Tissue. Ii. J. Cell Biol. 1963; 19:33–44. [PubMed: 14069800]

Raaijmakers MH, Mukherjee S, Guo S, Zhang S, Kobayashi T, Schoonmaker JA, Ebert BL, Al-Shahrour F, Hasserjian RP, Scadden EO, et al. Bone progenitor dysfunction induces myelodysplasia and secondary leukaemia. Nature. 2010; 464:852–857. [PubMed: 20305640]

Rodda SJ, McMahon AP. Distinct roles for Hedgehog and canonical Wnt signaling in specification, differentiation and maintenance of osteoblast progenitors. Development. 2006; 133:3231–3244. [PubMed: 16854976]

Sacchetti B, Funari A, Michienzi S, Di Cesare S, Piersanti S, Saggio I, Tagliafico E, Ferrari S, Robey PG, Riminucci M, Bianco P. Self-renewing osteoprogenitors in bone marrow sinusoids can organize a hematopoietic microenvironment. Cell. 2007; 131:324–336. [PubMed: 17956733]

Schindeler A, McDonald MM, Bokko P, Little DG. Bone remodeling during fracture repair: The cellular picture. Semin. Cell Dev. Biol. 2008; 19:459–466. [PubMed: 18692584]

Sipkins DA, Wei X, Wu JW, Runnels JM, CÔté D, Means TK, Luster AD, Scadden DT, Lin CP. In vivo imaging of specialized bone marrow endothelial microdomains for tumour engraftment. Nature. 2005; 435:969–973. [PubMed: 15959517]

Walkley CR, Olsen GH, Dworkin S, Fabb SA, Swann J, McArthur GA, Westmoreland SV, Chambon P, Scadden DT, Purton LE. A microenvironment-induced myeloproliferative syndrome caused by retinoic acid receptor gamma deficiency. Cell. 2007a; 129:1097–1110. [PubMed: 17574023]

Walkley CR, Shea JM, Sims NA, Purton LE, Orkin SH. Rb regulates interactions between hematopoietic stem cells and their bone marrow microenvironment. Cell. 2007b; 129:1081–1095. [PubMed: 17574022]

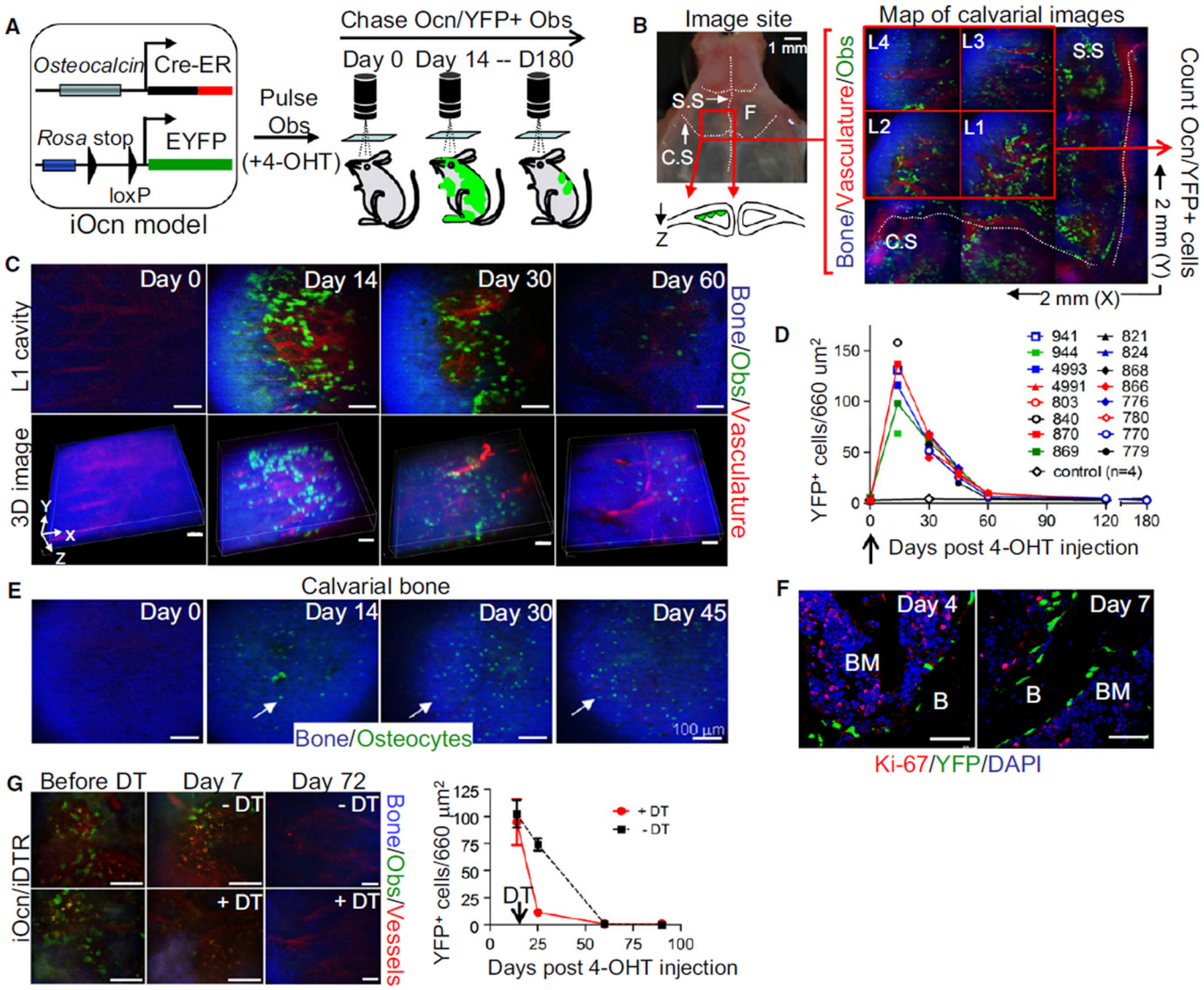

Figure 1. Mature *osteocalcin*$^+$ Osteoblasts Turn Over Rapidly In Vivo without Evidence of Proliferation

(A) Preexisting osteoblasts were pulsed and chased using a transgenic mouse (iOcn mouse). YFP was induced by tamoxifen (4-OHT) injection (2 doses) at 4–6 weeks of age and Ocn/YFP$^+$ osteoblasts were tracked by in vivo imaging at the indicated time points.

(B) Intravital microscopy was used to scan a 2 mm × 2 mm region (X, Y) of mouse calvarial cavity (red box, left panel and magnification in right panel) in left frontal bone (F) near the intersection of the coronal (C.S.) and sagittal (S.S.) sutures (left). Bone collagen (blue), Ocn/YFP$^+$ osteoblasts (green), and vasculature (red) in scanned area were mapped by acquiring a 3 × 3 grid of 3D stacks (X, Y, Z: 660 μm × 660 μm × 100 μm in depth). Four red boxes (L1–L4; 660 μm^2 each) represent the site of image analysis over time. Diagram represents a simplistic cross section view of the calvarial cavity.

(C) Ocn/YFP$^+$ osteoblasts in L1 position of the same iOcn mouse were tracked at the indicated time points (top). Z-stack images (50–100 μm depth) were reconstructed for 3D image analysis (bottom).

(D) The average number (L1–L4) of Ocn/YFP$^+$ osteoblasts from different mice were plotted at the indicated times. Each symbol represents an individual mouse (n = 16, control; n = 4).

(E) Ocn/YFP-labeled osteocytes within superficial calvarial bone from the same mouse in Figure 1C were imaged at several time points.
(F) Proliferation of Ocn/YFP$^+$ osteoblasts (YFP, green) was assessed four (Day 4) or seven (Day 7) days after 4-OHT treatment in the calvarial cavity of iOcn mice by anti-Ki-67 immunohistochemistry (Ki-67, red). Anti-GFP/YFP staining was used for enhancing YFP signal. Blue, DAPI.
(G) Mature osteoblasts in the calvaria of iOcn/iDTR mice imaged at 14 days (Before DT) or after three daily doses (100 μg/dose) of diphtheria toxin (+DT) or PBS as a control (−DT). The number of labeled osteoblasts was sequentially tracked by intravital microscopy at the indicated time points. Representative consecutive images (left) and the average numbers of osteoblasts in 4–6 images (660 μm^2/each) per mouse (n = 3/group) (right) are shown.
Scale bars are 50 μm (F) or 100 μm (C, E, and G). Data represent at least three independent experiments (F). See also Figure S1.

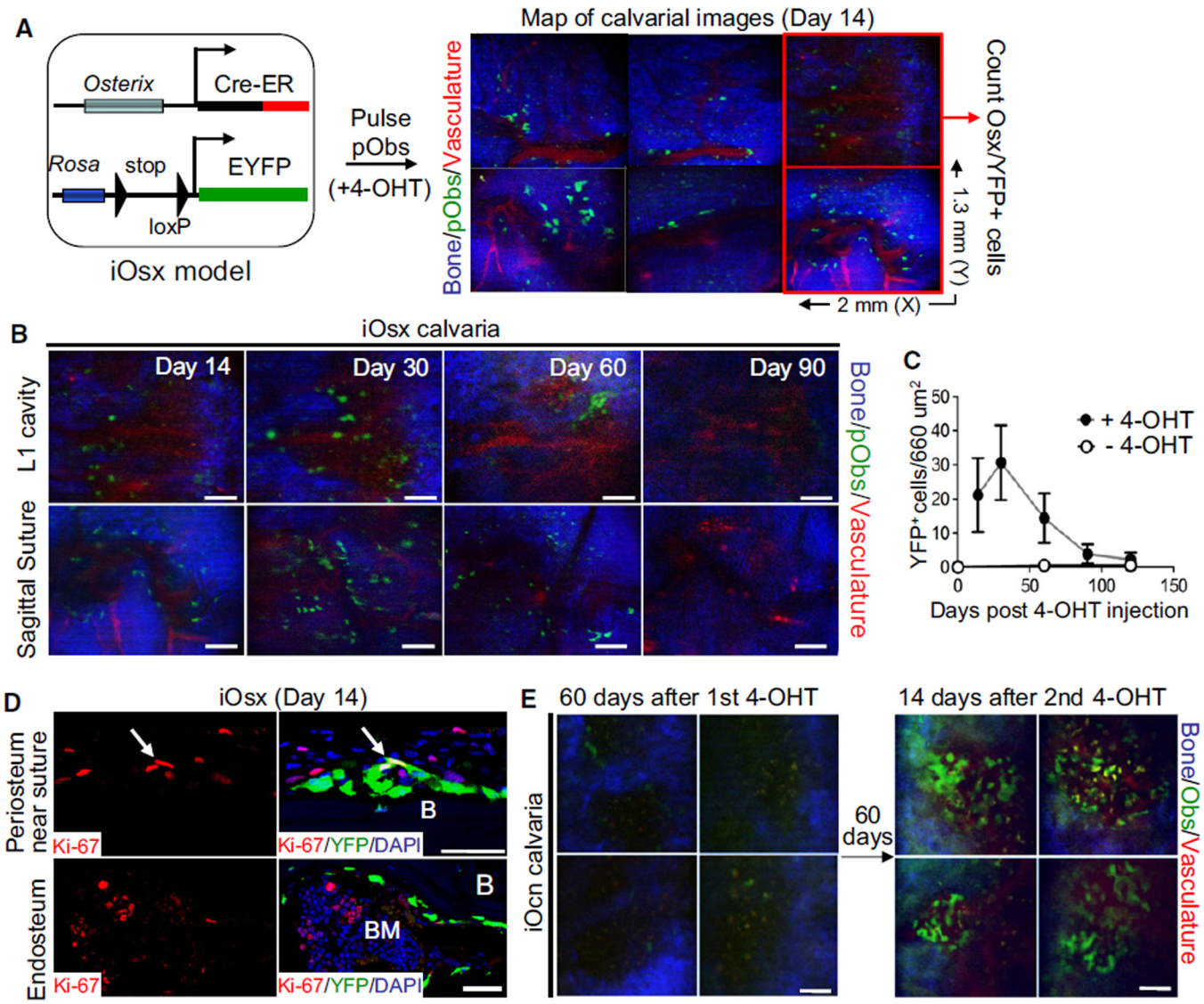

Figure 2. *Osterix*$^+$ Preosteoblasts Turn Over Rapidly In Vivo without Evidence of Proliferation

(A) Sequential imaging of *Osterix*$^+$ preosteoblasts in iOsx mice induced with tamoxifen (+4-OHT) by injection at 4–6 weeks of age. Osx/YFP$^+$ preosteoblasts were tracked by in vivo imaging. Scanned area covering the calvarial cavity and sagittal suture in the left frontal bone was mapped by acquiring a 3 × 2 grid of 3D stacks (X, Y, Z: 2 mm × 1.3 mm × 100 μm in depth). Two red boxes (660 μm^2 each) represent the site of image analysis for tracing the number of preosteoblasts over time. Bone collagen (blue), Osx/YFP$^+$ preosteoblasts (green), and vasculature (red) are shown.

(B and C) *Osx*-induced preosteoblasts were tracked at the indicated time points by sequential imaging. The average numbers of *Osx*-induced preosteoblasts from different mice with (black circle, n = 10) or without (white circle, n = 4) 4-OHT treatment were plotted at the indicated times (C). Error bars, ± SD.

(D) Proliferation of *Osx*-induced preosteoblasts on the periosteum near a suture (top) or on the endosteal surface (bottom) was assessed by anti-Ki-67 immunohistochemistry (red) fourteen days after 4-OHT treatment. Arrows indicate YFP and Ki-67 double-positive cells (yellow).

(E) Continuous replacement of osteoblasts by new osteoblasts was assessed in iOcn mice 60 days after the first tamoxifen administration (left) and maintained for an additional 60 days. Newly labeled osteoblasts in the same position were reimaged at 14 days after the second tamoxifen administration (right) (n = 4).

Scale bars are 20 μm (D) or 100 μm (B and E). Data represent three independent experiments with similar results (D). See also Figure S2.

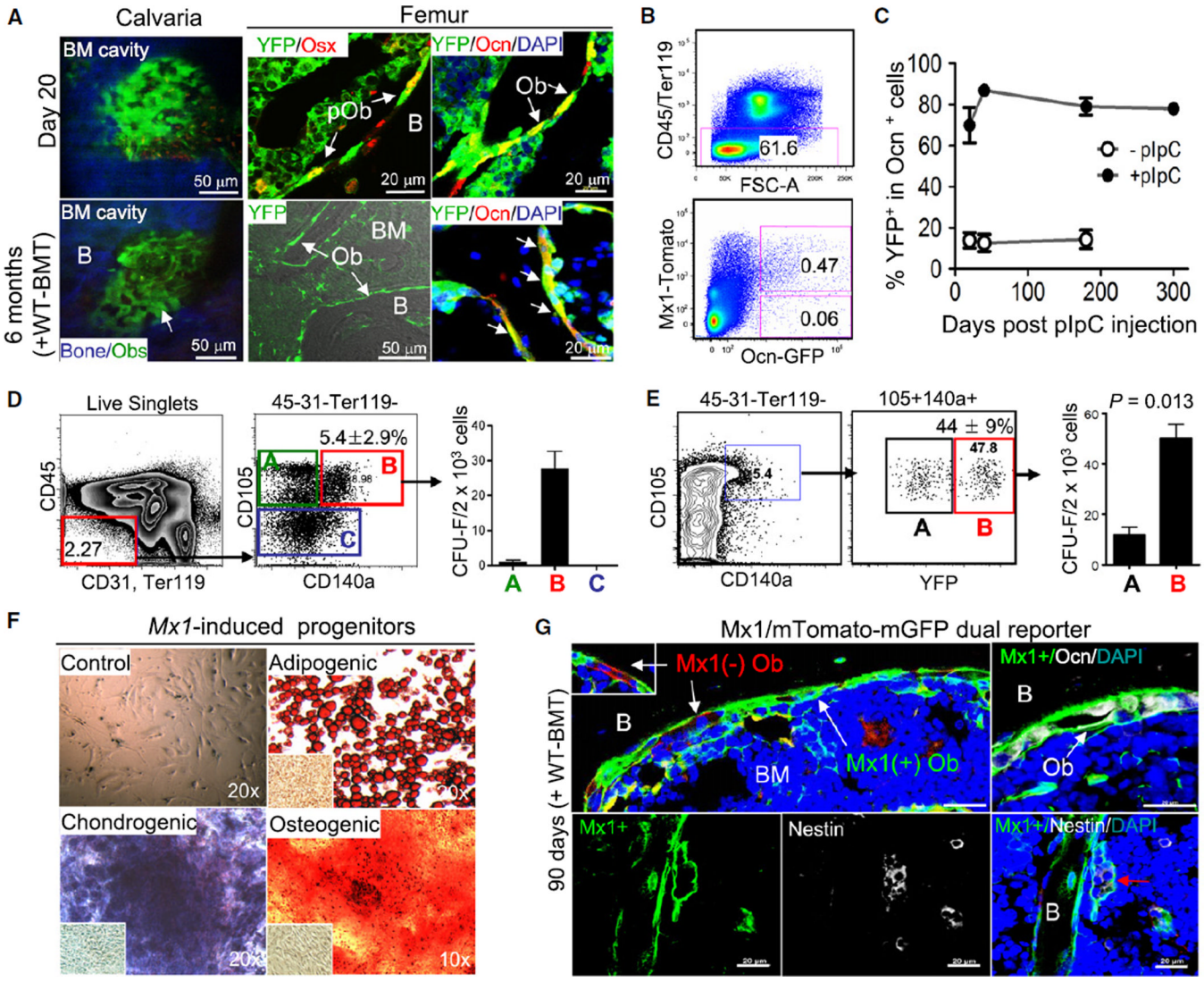

Figure 3. *Mx1*-Induced Cells Have MSC Characteristics and Maintain Long-Term Repopulation of Osteoblasts In Vivo

(A) *Mx1*-induced osteogenic cells (YFP^+) in calvaria (left) or femur sections (middle and right) of Mx1/YFP mice prepared 20 days after pIpC treatment (day 20) or 6 months after pIpC treatment (at 6–8 weeks after irradiation and wild-type bone marrow transplantation, +WT-BMT) were analyzed by undergoing intravital microscopy (left, blue, bone; green, *Mx1*-induced osteoblasts) or by being stained with anti-GFP/YFP (YFP), anti-osterix (Osx, for preosteoblasts), and anti-osteocalcin (Ocn, for mature osteoblasts) antibodies (right).

(B) Labeling efficiency of osteoblasts by *Mx1*. From collagenase-treated bones of Mx1/Tomato/Ocn-GFP trigenic mice at 30 days after pIpC treatment following WT-BMT, the percentage of *Mx1*-induced ($Tomato^+GFP^+$) or noninduced (GFP^+) osteoblasts was analyzed by flow cytometry.

(C) Percentage of *Mx1*-induced osteoblasts (YFP^+Ocn^+) before (−pIpC) or after pIpC (+pIpC) treatment as analyzed by anti-GFP/YFP, anti-osteocalcin immunohistochemistry, and FACs of cells from femurs at the indicated time points (n = 5 per group, right panel).

(D) Enrichment of clonogenic stromal cells in the $CD105^+CD140a^+$ fraction. From collagenase-treated wild-type bone cells, the nonhematopoietic fraction ($CD45^-CD31^-Ter119^-$) was further separated with CD105 and CD140a. Indicated fractions

(A, B, and C) were sorted and their clonogenicity was analyzed by CFU-F assays (>50 cells/colony at 14 days) (right, n = 5).

(E) *Mx1*-induced labeling in Mx1/YFP mice was examined using the same antibodies and analyzed as in Figure 3D. The percentage of YFP^- (box A) and YFP^+ (box B) within $CD105^+CD140a^+$ cells was determined and these fractions were used for CFU-F assays (right, n = 4).

(F) Multilineage differentiation potential of *Mx1*-induced clones was examined using single-cell-driven, clonally expanded *Mx1*-induced progenitors (Figure 3E, box B) that were further incubated with indicated condition medium or MSC medium (Control) for 28 days (n = 8). Cells were stained with Oil-Red for adipocytes (Adipogenic), Alizarin-Red for osteoblasts (Osteogenic), or Toluidine-blue for chondrocytes (Chondrogenic). NIH 3T3 fibroblasts cultured with conditioned medium were stained as a control (inserted images).

(G) Eight weeks after lethal irradiation followed by wild-type marrow transplantation (WT-BMT), Mx1/mTmG mice were treated with five doses of pIpC every other day. After 90 days of further tracing, *Mx1*-induced ($mGFP^+$, green) or *Mx1*-noninduced ($mTomato^+$, red) osteoblasts from femur sections were analyzed by anti-osteocalcin (top right) or by anti-nestin immunohistochemistry (bottom). Red arrow indicates *Mx1* and nestin double positive cells. Bone (B), bone marrow (BM), and osteoblasts (Ob) are indicated. Blue, DAPI (A and G).

Numbers in the histogram indicate the average of 5–10 different analyses; error bars, ± SD (D and E). Scale bars are 20 μm (G). Data represent more than three independent experiments with comparable results (A and G). See also Figures S3 and S4.

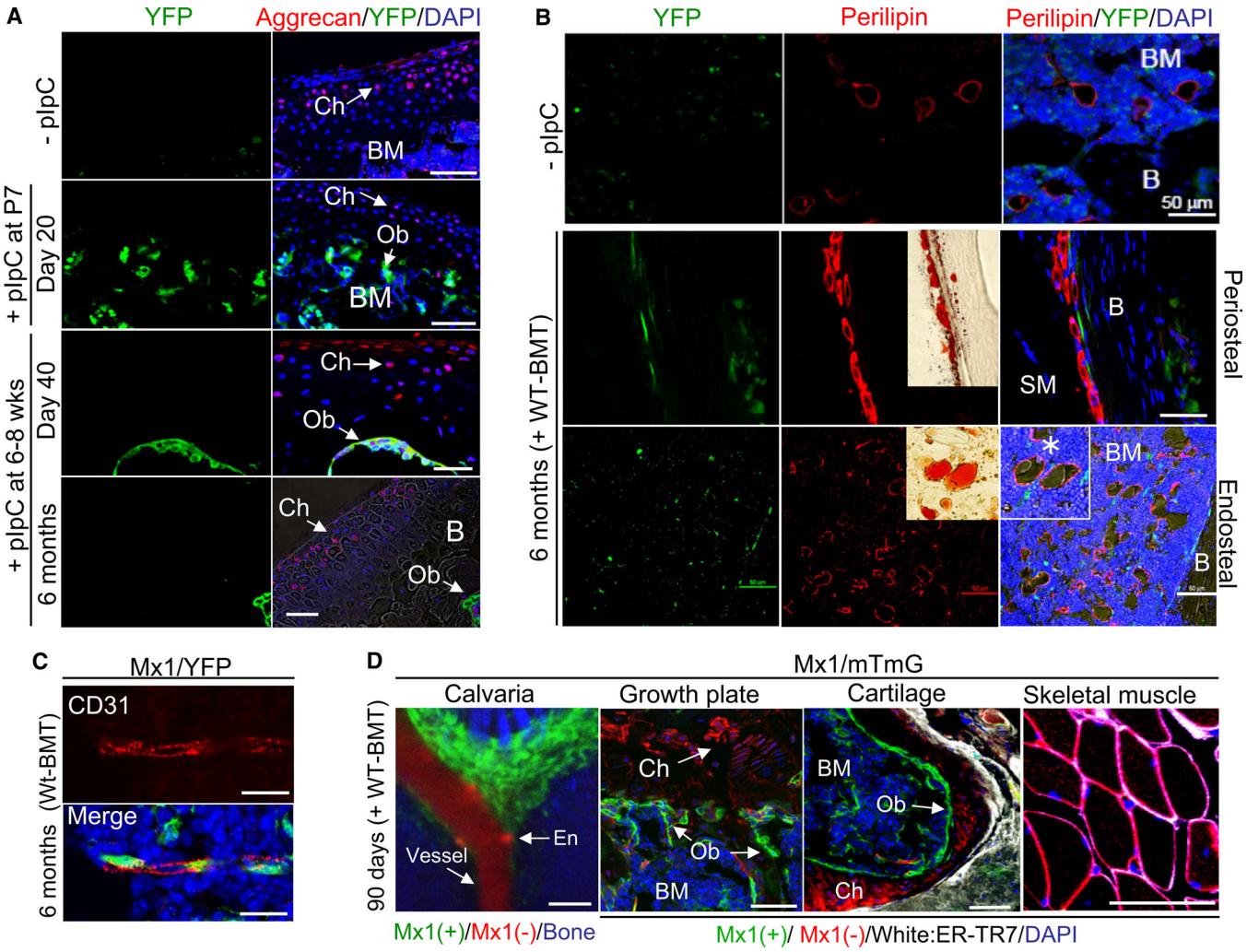

Figure 4. *Mx1*-Induced Cells Are Osteogenic Stem/Progenitors and Do Not Contribute to the Maintenance of Other Bone Marrow Mesenchymal Cells In Vivo

(A) Femurs from recipient Mx1/YFP mice transplanted with wild-type bone marrow were analyzed before (−pIpC) or 20 days after 5 doses of pIpC from postnatal day 7 (+ pIpC at P7), and 40 days (day 40) or 6 months after five doses of pIpC at 6–8 weeks old (6 months + WT-BMT) for *Mx1*-induced progenitor contribution to chondrocytes (Ch) in articular cartilage. Sections were stained by anti-GFP/YFP and anti-Aggrecan antibodies (red), respectively. BM, bone marrow; B, bone; Ob, osteoblasts.

(B) *Mx1*-induced progenitor contribution to adipocytes in outer surface (periosteal) or marrow (endosteal) of bones was assessed by immunostaining of femur sections with anti-GFP/YFP (green) and anti-perilipin antibody (red) and by Oil-Red staining (inserted images). Bones (B), bone marrow (BM), and skeletal muscle (SM) were indicated. Asterisk indicates adipocytes with lipid droplets.

(C) *Mx1*-induced progenitors are perivascular and distinct from endothelial cells. Sections from Figure 4D were stained by anti-GFP/YFP (green) and anti-CD31 (red) antibodies.

(D) By using dual reporter mice (mTmG) crossed with *Mx1-cre* mice, $Mx1^{+}$ (green) or $Mx1^{-}$ (red) cells were analyzed by intravital microscopy of the calvaria (left) or by immunohistochemistry of femur sections (Growth plate and Cartilage) and skeletal muscle. Bone marrow (BM), chondrocyte (Ch), osteoblast (Ob), vessel, and endothelial cells (En)

are indicated. To distinguish fibroblasts, anti-ER-TR7 staining (white) was included. Blue, DAPI (A–D).

Scale bars are 20 μm (C) or 50 μm (A, B, and D). All data represent at least two (A, −pIpC) or three independent experiments with consistent results. See also Figure S5.

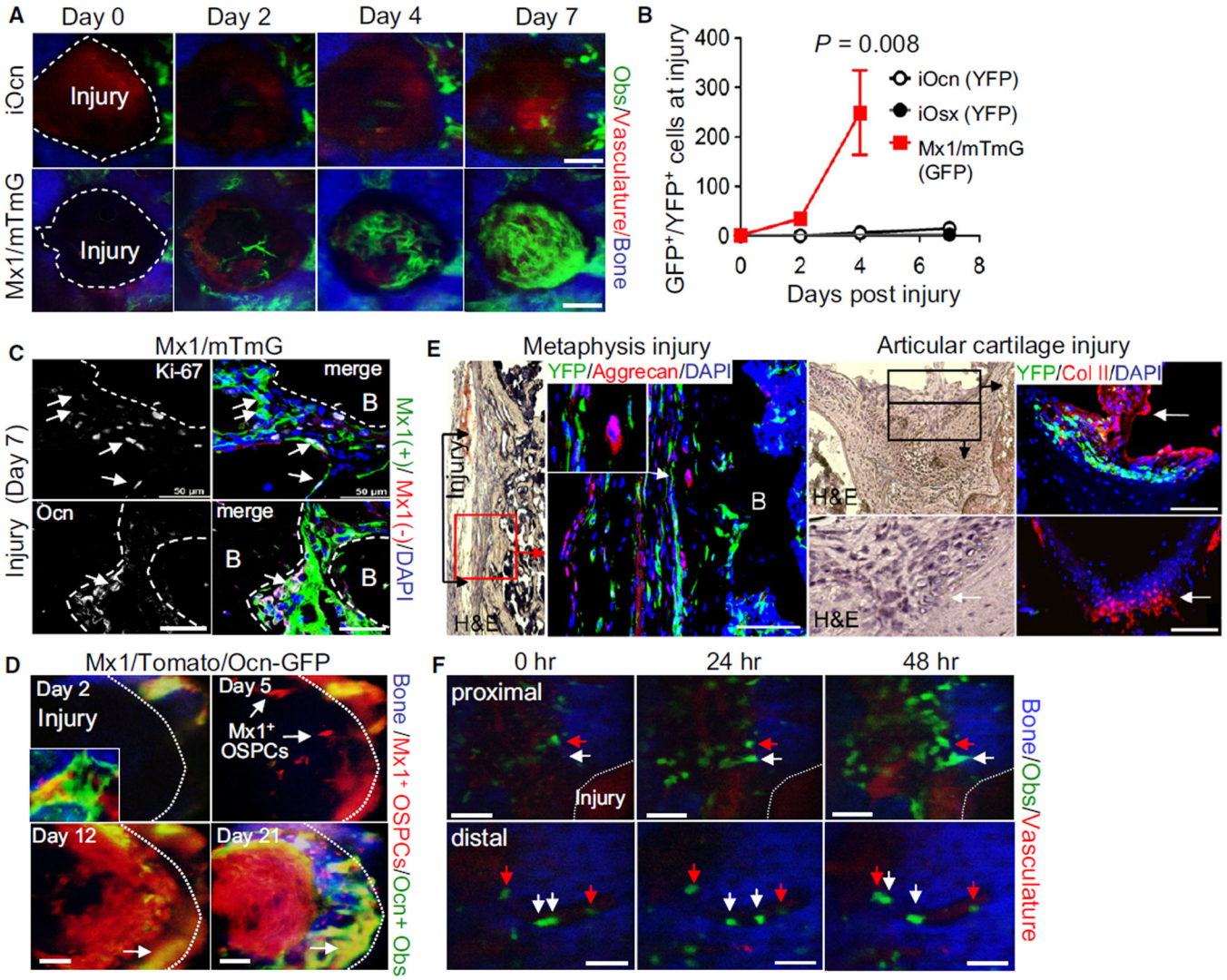

Figure 5. Migration and Proliferation of *Mx1*-Induced OSPCs, but Not Differentiated Osteoblasts, Supply the Majority of Osteoblasts in Fracture Healing

(A) Dramatic relocation of *Mx1*-induced OSPCs during fracture healing. YFP$^+$ osteoblasts near the injury on iOcn (top) or Mx1/mTmG mouse calvaria (bottom) were imaged immediately after injury (day 0) and at the indicated times after injury.

(B) The average numbers of *Ocn*-, *Osx*- or *Mx1*-labeled cells within the injury zone were plotted at the indicated time (n > 5 per group). Error bars, ± SD.

(C) *Mx1*-induced OSPCs were assessed for proliferation by Ki-67 staining (white, top) and differentiation by anti-Ocn (white, bottom) seven days after injury from Figure 5A. Arrows indicate *Mx1* and Ki-67 double positive cells (top) and *Mx1* and *Ocn* double positive osteoblasts (bottom). Green, *Mx1*+ cells; red, *Mx1*- cells; white, Ki-67+ (top) or Ocn+ (bottom) cells; blue, DAPI.

(D) *Mx1*-induced OSPCs and osteoblasts at the injury site on Mx1/Tomato/Ocn-GFP mouse calvaria were imaged at the indicated times after injury. An image in the bottom left corner of the day 2 image indicates osteogenic cells in uninjured bone. Arrows indicate newly translocated *Mx1*-induced OSPCs (day 5, red) and osteoblasts derived from *Mx1*$^+$ OSPCs (day 12 and day 21, yellow). Blue, bone.

(E) Three weeks after injury at distal metaphysis (left) and articular cartilage (right) of femurs in Mx1/YFP mice, *Mx1*-induced cells and chondrocytes at the site of microfractures were assessed by immunostaining with anti-GFP/YFP, anti-aggrecan (left), and anti-collagen type II (right, Col II) antibodies and by H&E staining of parallel sections. White arrows indicate newly generated chondrocytes. B, bone.
(F) Mature osteoblasts assessed for mobility after injury. At 14 days after tamoxifen treatment, Ocn/YFP$^+$ osteoblasts were imaged immediately (0 hr) or 24 hr and 48 hr after injury near (proximal; <400 μm) or over 400 μm away (distal) from the injury site. Arrows indicate stationary (red) and migrating (white) osteoblasts. Blue, bone; green, YFP$^+$ osteoblasts; red, vasculature (Q-dots).
Scale bars are 50 μm (C–F) or 100 μm (A). Data represent three (C and E) or five (A, D, and F) independent experiments (two to four injuries/each experiment) with comparable results. See also Figure S6.

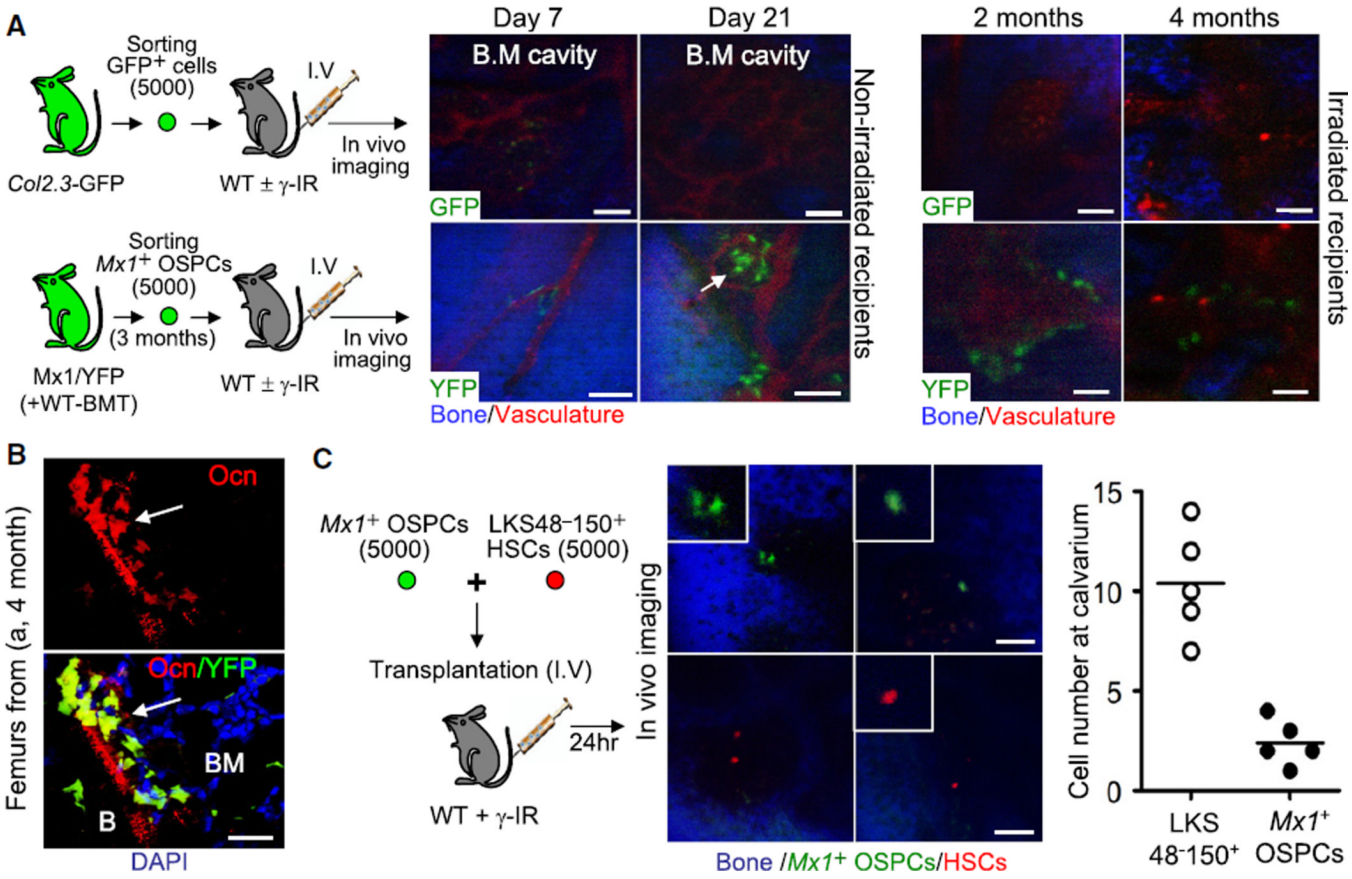

Figure 6. *Mx1*-Induced OSPCs Are Transplantable by Intravenous Infusion

(A) Sorted *Mx1*-induced osteogenic stem/progenitors (bottom, 5,000 $Mx1^+$ OSPCs from Figure 3E, box B) or control osteoblasts (top, 5,000 GFP^+ cells from *Col2.3-GFP* mice) were transplanted intravenously into wild-type mice and were tracked in vivo by intravital microscopy at indicated time points (n = 3 to 5 mice per each group).

(B) Osteoblast differentiation of transplanted $Mx1^+$ OSPCs in femur sections from (A) (4 months) was tested by anti-osteocalcin staining (n = 3).

(C) Relative homing efficiency of *Mx1*-induced osteogenic stem/progenitors. Sorted $Mx1^+$ OPCs (5,000) and wild-type $Lin^-Kit^+Sca^+CD48^-CD150^+$ HSPCs (5,000) stained with DiD (red) were mixed and transplanted intravenously into wild-type irradiated mice. Twenty-four hours later, the number of cells in bone marrow of calvaria was counted by intravital microscopy.

An arrow in (A) indicates $Mx1^+$ OSPCs in the bone marrow cavity. Scale bars are 20 μm (B) or 100 μm (A and C). Arrows in (B) indicate differentiated osteoblasts from donor cells. See also Figure S7.

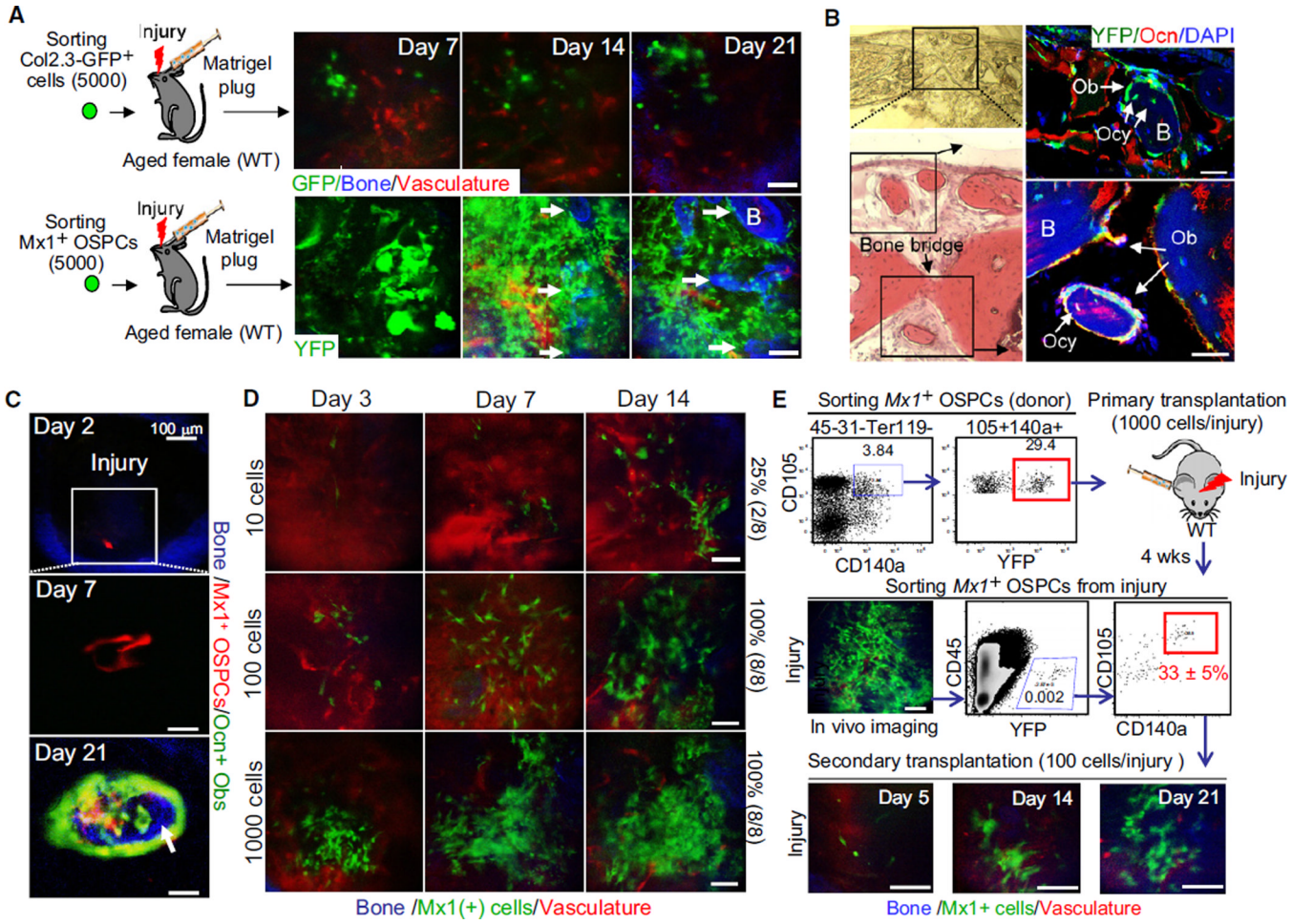

Figure 7. *Mx1*-Induced OSPCs Contribute to Fracture Healing

(A) The same 5,000 *Mx1*$^+$ OSPCs (bottom) or Col2.3-GFP$^+$ osteoblasts (top) from Figure 6A were mixed with 20 μl of matrigel and transplanted at the site of calvarial injury (~1 mm diameter) of ~1-year-old wild-type female mice (Aged female). Transplanted cells and new bone formation were tracked by sequential in vivo imaging.

(B) Osteoblast differentiation and new bone formation of transplanted *Mx1*-induced OSPCs at injury sites (day 21) was assessed by bright field (top left), H&E (bottom left), and anti-osteocalcin staining (right). Black boxes indicate the sites of newly generated bones by *Mx1*$^+$ osteoblasts (Ob) and *Mx1*$^+$ osteocytes (Ocy) derived from transplanted *Mx1*$^+$ OSPCs.

(C) A single *Mx1*-labeled OSPC from Mx1/Tomato/Ocn-GFP mice was transplanted into the calvarial injury of a wild-type mouse. Clonal expansion, osteogenic differentiation (Tomato$^+$GFP$^+$), and new bone formation (arrow, blue) were assessed by sequential in vivo imaging at the indicated times.

(D) Engraftment frequency of *Mx1*$^+$ OSPCs in injury was tracked by sequential in vivo imaging. Numbers at left are input cell number and the frequency of successful engraftment shown at the right.

(E) Serial transplantation of *Mx1*$^+$ OSPCs. Sorted *Mx1*$^+$ OSPCs (red box on top scatterplot, 1,000 cells/injury, n = 8) were transplanted into injury sites of C57BL/6 recipients. Four weeks later, cells from the injury site were analyzed by in vivo imaging (middle, left), FACs-sorted (red box in middle right scatterplot), and retransplanted into secondary recipients (100 cells/injury, n = 3). The repopulation of *Mx1*$^+$ OSPCs at secondary injuries was tracked by sequential in vivo imaging at indicated time points (bottom).

Arrows in (A) and (C) indicate newly developed bones. Scale bars are 20 μm (B), 50 μm (C, D, and E), or 100 μm (A). Data represent 12 injuries (A) or three (C) independent experiments with comparable results.